Influence of Lanthanum concentration on the Corrosion Behaviour of Binary Mg-La Alloys

Rosario Silva Campos, Daniel Höche, Carsten Blawert, Karl Ulrich Kainer

GKSS Research Centre, Institute of Materials Research, Max-Planck-Straße 1, Geesthacht 21502, Germany

Keywords: Magnesium corrosion, Rare earth - Lanthanum, XPS, Auger

Abstract

Different contents of Lanthanum have been added to Magnesium and have been investigated on their influence on the microstructure and the corrosion properties. The microstructure was studied by optical microscopy. Corrosion performance was evaluated using potentiodynamic polarization measurements. Immersion tests were carried out using distilled water and 0.1 M sodium chloride solution. The corrosion products were investigated by X-ray induced photoelectron spectroscopy (XPS), Auger electron spectroscopy (AES) and X-ray diffraction (XRD) which lead to detailed information on phase formation. The oxide and hydroxide formation have been correlated to the chemical states and formed intermetallics, i.e by taking into account the XPS peak shift and peak splitting of the the Mg-2p state. Additionally, the results have been verified by means of AES on the Mg-KLL, O-KLL and La-MNN excitation and by XRD. Latter suggests the supplemental formation of a nanocrystalline phase.

Introduction

Magnesium alloys are known for their good properties, which are greatly attractive to the automotive and aerospace industries. Their use however is limited due to their poor corrosion properties [1]. There are two main reasons of this lack of corrosion resistance [2]. Firstly, there is internal galvanic corrosion caused by second phases or impurities [3]. Secondly, the quasi-passive hydroxide film on Mg is much less stable than the passive films which form on metals such as aluminium and stainless steels. This quasi-passivity provides only poor pitting resistance for Mg and Mg-alloys [4]. The early Mg-alloys suffered rapid attack in moist conditions due mainly to the presence of impurities, notably iron, nickel, and copper. These impurities or their compounds act as minute cathodes in a corroding medium. They create micro-cells with an anodic Mg matrix [5].

Previous studies [6-9] have showed that for Mg alloys, rare earths (RE) elements can enhance their corrosion resistance. For example addition of Ce as a typical RE element prompts the formation of an Al- enriched layer on the corrosion film, which contributes to the corrosion resistance of AZ91D alloy [10]. In case of Mg-Gd-Zr alloys the addition of La or Ce reduces the dendrite arm spacing of the as- cast alloy and improves the mechanical properties and age hardening response [11].

In this work several experiments were performed in order to study the corrosion behaviour of Mg-La alloys. The immersion test, potentiodynamic polarization and analytical techniques were combined to study the characteristics of the films formed on the surface of Mg-La specimens immersed in different corrosion environments.

Experimental Procedure

Casting

Several Mg-La alloys were prepared from their pure elements, amounts in weight percent were added (1, 5, 10 and 15 wt% La) and balance with high purity Mg. The alloys were casted in a resistance furnace at a starting temperature of 700°C under an Argon-SF6 atmosphere. After casting, chemical analysis was performed in order to ensure the composition homogeneity in the whole specimen.

Optical Characterization

The samples were grinded with SiC paper up to grit 4500; polished with SiO_2 and etched with a picric acid solution, ultrasonically cleaned using ethanol, and dried in hot air. After the pre-treatment the surfaces were investigated using a light microscope - PC system including metallographic software.

Immersion

Flat specimens with dimensions 20 x 15 x 4 mm³ were cut using a diamond cutting disc, grinded with SiC paper up to grit 1200, ultrasonically cleaned using ethanol and dried in hot air. The coupons were immersed 10 days in deionised water. Subsequently these were washed with ethanol and dried in hot air. The samples were used for XPS analysis. Pure Mg samples were treated in the same way to compare the results.

Electrochemical Measurements

The coupons were cut from the cast ingot to the following dimensions 20 x 15 x 10mm³, grinded with SiC paper up to grit 1200, ultrasonically cleaned using ethanol and dried in hot air. The electrochemical tests were conducted in an acrylic cell (330 ml electrolyte) using a Gill AC Potentiostat from ACM Instruments. The working electrode had ~0.5 cm² exposed area. A solution of 0.1 M NaCl was used as electrolyte, while reference and auxiliary electrodes were Ag/AgCl, and Pt grid respectively. The experiments were done at 25°C without deareation. Magnetic stirring was performed with a 4 cm length magnet at low speed. Experiments were carried out in triplicate. The sequence of measurements used was (a) 2 hours of open circuit potential followed by (b) potentiodynamic scanning starting at -200 mV relative to OCP and ending at 1500 mV and current limit was 0.5 mA/cm² with a scan rate of 0.5 mV/s. The corrosion density was determined from the current density at the intersection of cathodic slope with the vertical line through the OCP.

X-ray induced Photoelectron Spectroscopy (XPS)

XPS experiments were carried out on a Kratos Axis Ultra DLD attached with a 15 kV X-ray gun using monochromatic Al K_α radiation. The spot size was 700 x 300 microns and the pass energy 40 eV at the regions measurements. Due to physical limits the information depth is limited to approx. 5 nm. Additionally, argon ions (4 keV) have been used to etch the samples in order to

obtain depth profiles. The used sputter rate was approx. 40 nm per minute for total sputter times of 250 min.

Auger Electron Spectroscopy (AES)

AES is an attached feature of the Kratos system. An electron gun having a spot size of about 100 nm and a beam current of 5 nA has been focussed on points of interests, which were analyzed at specific kinetic energies.

X-ray diffraction (XRD)

The measurements have been performed on a Panalytical system including a poly-capillary optic and an "Euler" circle using CuK_α radiation. The scans have been carried out at Bragg-Brentano geometry leading to an information depth of about 200 microns.

Results and Discussion

Microstructures of Mg alloys with different La compositions are shown in Fig. 1. In all cases two phases are present. Primary phase is α–Mg and second phase or eutectic corresponds to (α-Mg+ $Mg_{17}La_2$) (XRD data is shown in Fig. 7).At the highest compositions (Fig 1c and 1d), the α–Mg regions are smaller and are fully enveloped by the eutectic. The lamellar structure of the eutectic phase becomes also coarser as the La content increases.
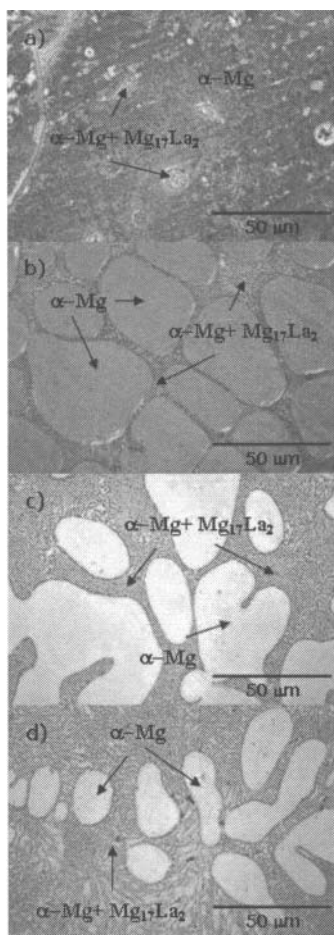

Figure 1. Microstructure of Mg-La alloys a) Mg1wt%La, b)Mg5wt%La, c) Mg10wt% La and d) Mg15wt% La

Electrochemical Tests

The corrosion potentials (Open circuit potential.) of Mg-La alloys were recorded for 2 hours. The potential evolution is shown in Fig. 2 and the potentials measured after 2 hours are reported in Table 1. Mg, Mg1La, Mg5La have similar potentials and are more active than the rest, while Mg-La$_{intermetallic}$ ($Mg_{17}La_2$), Mg10La and Mg15La alloys have more noble potentials than Mg but are more active compared to La. With increasing La content the potential shifts to more noble values which are consistent with the nobler potential of La compare with Mg.
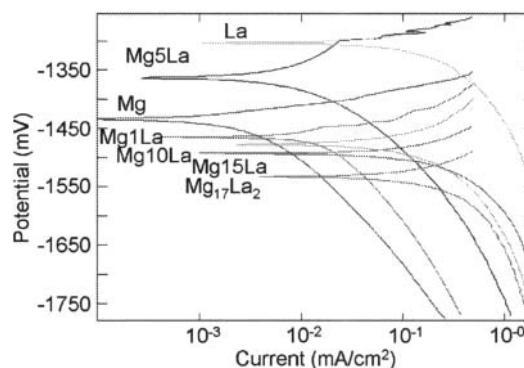

Figure 2. Potentiodynamic current-potential curves in 0.1 M NaCl at T_{amb} (pH=7 with stirring)

Table I. Electrochemical corrosion data for the alloys in 0.1M NaCl at T_{amb} (pH=7 with stirring)

Alloy	OCP (2h) [mV]$_{Ag/AgCl}$	E_{corr} [mV]$_{Ag/AgCl}$	I_{corr} [μA/cm^2]	Corrosion Rate [mm/year]
Mg1La	-1572 ± 2	-1464 ± 10	22.5 ± 1	0.51 ± 0.02
Mg5La	-1573 ± 2	-1364 ± 4	27.3 ± 20	0.62 ± 0.39
Mg10La	-1552 ± 10	-1477 ± 12	160 ± 32	3.67 ± 0.74
Mg15La	-1511 ± 1	-1492 ± 3	275 ± 56	3.70 ± 1.29
Mg$_{pure}$	-1576 ± 4	-1433 ± 11	4.6 ± 1.6	0.11 ± 0.04
Mg$_{17}$La$_2$	-1549 ± 2	-1533 ± 6	182 ± 44	4.15 ± 1.00
La$_{pure}$	-1330 ± 3	- 1303 ± 4	125 ± 8	3.06 ± 0.21

The current-voltage curves for the alloys are shown in Fig. 2 and the corrosion parameters are reported in Table 1. The microstructure changes due to La addition (Fig. 1) create variations on the corrosion resistance as shown in Fig. 3 and Table 1. Mg had the lowest corrosion rate value and additions up to 5 wt% La caused minor increase, while that with 10 wt% La or more causes a high increase on the corrosion rate. In other words, the eutectic phase (α-Mg + $Mg_{17}La_2$) gets more easily and rapidly corroded than the primary (α-Mg) phase. There are two main reasons to explain that behaviour. If the material is polarised, the potentials of Mg and $Mg_{17}La_2$ shift differently. The consequence is that in contrast to OCP the Mg matrix becomes more noble. In galvanic couple now the intermetallic is dissolving protecting the matrix. Furthermore the corrosion resistance of the intermetallic is low, thus with increasing La content in the alloy more of the eutectic forms with poor corrosion resistance which is additionally polarised anodically by the Mg matrix.
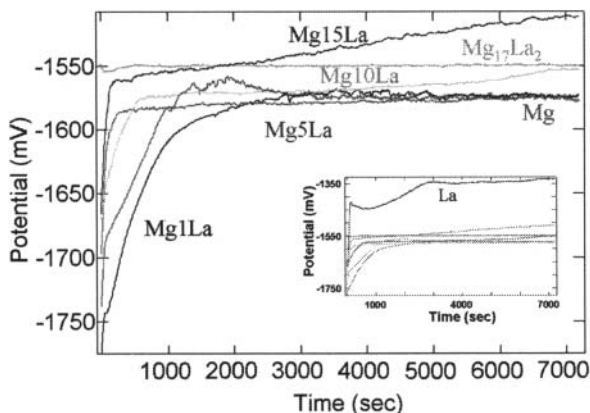
Figure 3. Open circuit potential vs time curves of the studied magnesium alloys in 0.1 M NaCl (pH=7) with stirring. Potentials are referred to Ag/AgCl electrode.

X-ray induced Photoelectron Spectroscopy (XPS)

The detailed analysis of corrosion processes needs the knowledge of the composition in the corroded material, especially of the resulting corrosion layers. Thus, XPS was applied to measure elemental depth profiles in an alternating process of sputtering and measuring. Fig. 4.represents the elemental distribution of the Mg-La alloys after immersion in distilled water for ten days.
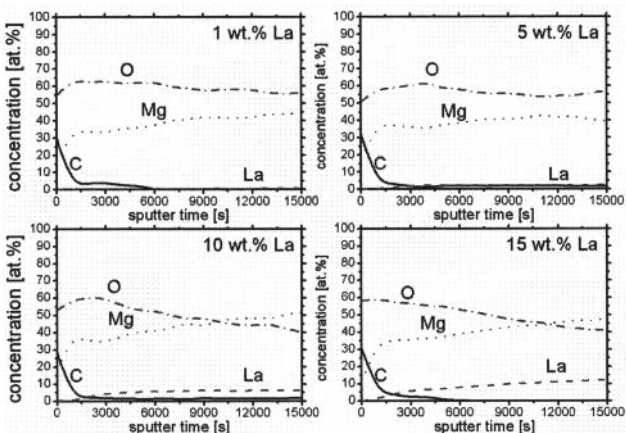

Figure 4. XPS depth profiles for Mg-La alloys measured by evaluating the peak areas of Mg 2p, O 1s, C 1s and La 3d states after different etch time steps.

First, it becomes visible that the carbon contamination is very similar for all samples. These C atoms are bonded in carbonates (mainly $MgCO_3$). As next it is obvious that the lanthanum content is very small close to the surface, which leads to the conclusion of a magnesium dominated process close to the surface. The Mg depth profiles (atomic content) are also very similar, but not the state of magnesium. This gets explained in the next paragraph. By means of the oxygen distribution it is possible to estimate the thickness of the corrosion layer. For higher La contents the layers are significantly thinner.

In order to get information on the chemical state inside of the corrosion layer, the Mg 2p state has been measured at a high resolution after sputtering. Fig. 5 shows the different atomic

bonds of magnesium for varying lanthanum weight contents. It has to be mentioned that the analyzed area is 700x300 µm², which yields in an average determination of the phases across the surface. The four high resolution scans reveal the different oxidation states of Mg-La alloys after immersion. For the lowest lanthanum content the typical hydroxide formation [12] occurs at least to the crater depth of that measurement. Additionally, after drying MgO phase formation occurs. The situation changes for higher La contents. Magnesium hydroxide formation gets suppressed due to the formation of $La(OH)_3$ (see X-ray diffraction), small amounts of La_2O_3 and a phase known as La_2MgO_x [13-14].
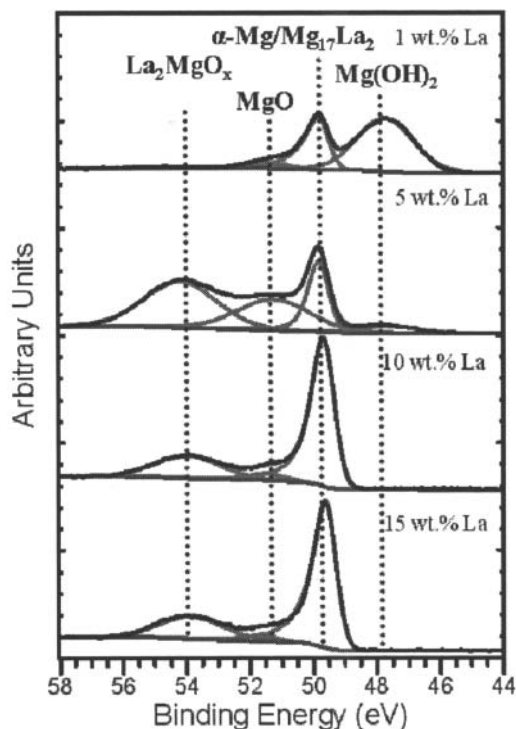

Figure 5. XPS high resolution scans of the Mg 2p state after completed etching. The corresponding chemical bond has been highlighted.

This corrosion behavior stays similar for higher La contents, but the layer thickness becomes thinner. As a result of the $Mg_{17}La_2$ intermettalic phase, La_2MgO_x formation seems to be the most common reaction product. It is interesting that this compound has catalytic properties especially with respect to CO_2 according to earlier studies in [13].

Auger Electron Spectroscopy (AES)

In order to verify the results detailed point analyses by means of auger spectroscopy was carried out for the 15wt.% lanthanum containing sample at the sputter crater. This allows studying the different atomic states at a very small localized area. In Fig. 6 some typical auger region scans of the Mg KLL, O KLL and the La MNNa excitation have been plotted, measured at the microstructure of the bulk and the intermettalic phase.

The corresponding Mg KLL transition at 1180 eV is related to the MgO phase [15] and the transitions in the O KLL auger spectra too [16]. Both spectra are convoluted by a weak signal related to

the La$_2$MgO$_x$ phase. There still not exists literature about auger spectra of this phase. Thus, it is very difficult to confirm this assumption, but the weak La MNNa excitation shows the existence of a small fraction of lanthanum at the measured point. According to the kinetic energies in [17] the La is in an oxidized state. Very interesting results arise from the studies at the intermetallic phase.
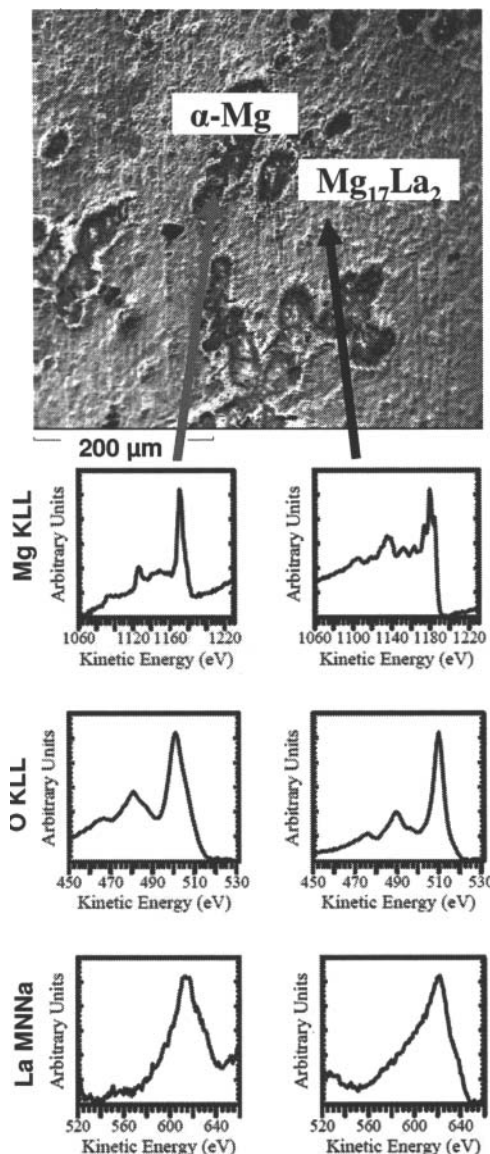

Figure 6. AES spectra of Mg, O and La excitations in different phases measured inside the sputter crater after completed etching for the Mg15La sample

The Mg KLL transition shows a strong peak splitting due to the interaction with the heavy lanthanum atoms at the Mg$_{17}$La$_2$ phase. At an energy of 1186 eV (the right shoulder) metallic magnesium has been detected [15]. Comparing the O KLL state to the bulk one another phase than MgO occurs. I can be assumed that the spectra is a convolution of La$_2$MgO$_x$, La$_2$O$_3$ and La(OH)$_3$ related

signals. Further studies are required for verification. The same problem exists for the evaluation of the La MNNa transition. The right shoulder at 634 eV also corresponds to the metallic phase [18], but there are no information available (also in the literature) to separate the oxidized state of lanthanum by means of auger electron spectroscopy..

X-ray diffraction (XRD)

XRD is one of the most powerful tools for material analyses also in this case. The diffraction patterns in Fig. 7 offer a lot of additional information on the corrosion process. All theta -2theta scans have been plotted by means of a logarithmic scale in order to see the pattern occurring from compounds close to the surface (information depth of corrosion products of approximately 5 μm). Otherwise the bulk signal (x-ray penetration depth about 200 μm) becomes dominant.
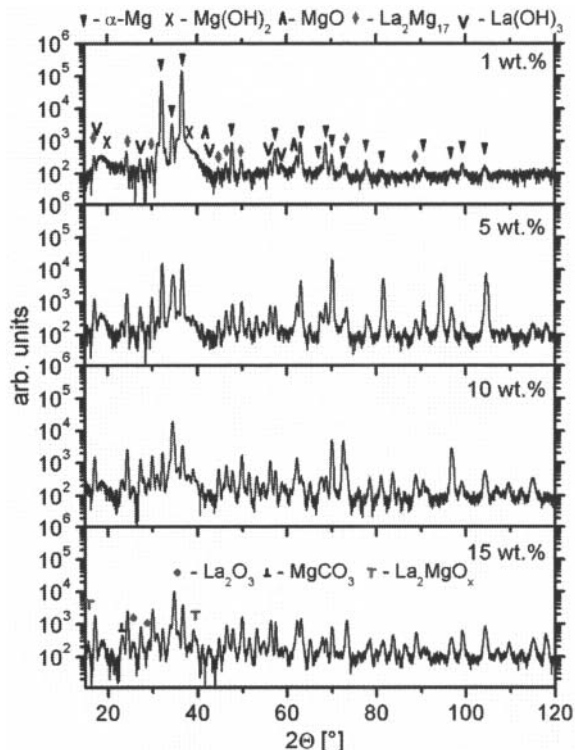

Figure 7. XRD pattern after corrosion tests using Bragg-Brentano scan geometry for different Mg-La alloys.

Obviously, a lot of different phases arise during the corrosion process, which complicates the evaluation due to peak convolutions. The strongest corresponding reflexes have been marked and labelled in Fig. 7 according to the ICDD database [19]. The ratio of α-Mg and Mg$_{17}$La$_2$ related peaks of the bulk material just verify the observations in the previous sections. It is conspicuous that the reflexes of both hydroxides (Mg, La) and of La$_2$MgO$_x$ are broadened. According to the theory (i.e. Debye-Scherrer) [20] such broadening occurs for a decreasing crystallite size. In the case of La$_2$MgO$_x$ a nanocrystalline microstructure would confirm the results in [13]. Besides, the typical oxides have been detected. The measurement of MgCO$_3$ is related to the strong carbon adsorption during the tests.

510

Conclusions

The presence of two phases: primary phase (α-Mg) and eutectic phase (α-Mg+ Mg$_{17}$La$_2$) will induce galvanic corrosion in Mg-La alloys. The corrosion rate depends strongly on the amount and distribution of these phases.

When the La content is higher than 5 wt% La, the alloys exhibit a potential even more noble than that of Mg, but the corrosion resistance decreases due to the increase of the eutectic phase.

For increasing lanthanum contents Mg(OH)$_2$ formation gets suppressed, but contrary La(OH)$_3$ formation becomes amplified. As a result the thickness of the corrosion layer is thinner. Besides the typical oxides are developing. It is likely that this has also a contribution to the decreasing corrosion resistance with increasing La content,

As next, a nanocrystalline La$_2$MgO$_x$ phase with catalytic properties has been formed. The influence on the corrosion process is still unclear.

References

1. G. Makar, J. Kruger and A. Joshi, *The effect of alloying elements on the corrosion resistance of rapidly solidified magnesium alloys*, International Magnesium Association and the Non-ferrous Metals Committee, The Minerals, Metals and Materials Society, Phoenix, 1988.
2. G. L. Makar and J. Kruger, "Corrosion studies of rapidly solidified magnesium alloys," *J Electrochem Soc,* 137 (2) (1990), 414-421.
3. E. Emley, *Principles of magnesium technology,* London, Pergamon Press, New York, 1966.
4. G. Makar and J. Kruger, *Corrosion of magnesium,* vol. 38, Maney Publishing, 1993.
5. I. Polmear, *Magnesium alloys,* Sevenoaks, UK 1989.
6. T. Takenaka et al., "Improvement of corrosion resistance of magnesium metal by rare earth elements," *Electrochimica Acta,* 53 (1) (2007), 117-121.
7. J. H. Nordlien et al., "Morphology and structure of water-formed oxides on ternary mgal alloys," *J Electrochem Soc,* 144 (2) (1997), 461-466.
8. F. Rosalbino et al., "Effect of erbium addition on the corrosion behaviour of mg-al alloys," *Intermetallics,* 13 (1) (2005), 55-60.
9. G. Song and D. St. John, "The effect of zirconium grain refinement on the corrosion behaviour of magnesium-rare earth alloy mez," *Journal of Light Metals,* 2 (1) (2002), 1-16.
10. Y. Fan, G. Wu and C. Zhai, "Influence of cerium on the microstructure, mechanical properties and corrosion resistance of magnesium alloy," *Materials Science and Engineering: A,* 433 (1-2) (2006), 208-215.
11. Q. Peng et al., "The effect of La or Ce on ageing response and mechanical properties of cast mg-gd-zr alloys," *Materials Characterization,* 59 (4) (2008), 435-439.
12. S. Ardizzone et al., "Magnesium salts and oxide: An xps overview," *Appl Surf Sci,* 119 (3-4) (1997), 253-259.
13. A. Ivanova, "Structure, texture, and acid-base properties of alkaline earth oxides, rare earth oxides, and binary oxide systems," *Kinetics and Catalysis,* 46 (5) (2005), 620-633.
14. J. M. Fraile et al., "The basicity of mixed oxides and the influence of alkaline metals: The case of transesterification reactions," *Applied Catalysis A: General,* In Press, Corrected Proof (-) (2010).
15. C. D. Wagner and P. Biloen, "X-ray excited auger and photoelectron spectra of partially oxidized magnesium surfaces: The observation of abnormal chemical shifts," *Surface Science,* 35 ((1973), 82-95.
16. J. C. Fuggle et al., "High-resolution auger spectra of adsorbates," *Journal of Electron Spectroscopy and Related Phenomena,* 26 (2) (1982), 111-132.
17. W. H. Hocking et al., "Scanning auger microscopy study of lanthanum partitioning in sphene-based glass-ceramics," *Philosophical Magazine A,* 49 (5) (1984), 637-656.
18. L. Davis et al., *Handbook of auger electron spectroscopy,* Physical Electronics Industries Eden Prairie, MN, 1976.
19. "Powder diffraction file," *ICDD,* International Centre for Diffraction Data, Newtown, PA,, 2008.
20. T. Ungár, "Microstructural parameters from x-ray diffraction peak broadening," *Scripta Materialia,* 51 (8) (2004), 777-781.